



# Identifying and understanding optical coherence tomography artifacts that may be confused with glaucoma

Identificando e compreendendo os artefatos de tomografia de coerência óptica que podem ser confundidos com o glaucoma

Ari Leshno<sup>1,2</sup> , Donald C. Hood<sup>3</sup> , Jeffrey M. Liebmann<sup>1</sup> , Carlos Gustavo De Moraes<sup>1</sup> 

<sup>1</sup> Bernard and Shirlee Brown Glaucoma Research Laboratory, Edward S. Harkness Eye Institute, Department of Ophthalmology, Columbia University Irving Medical Center, 635 W 165th St, New York, NY, USA 10032.

<sup>2</sup> Sackler Faculty of Medicine, Tel Aviv University, Tel Aviv, Israel.

<sup>3</sup> Department of Psychology, Columbia University Schermerhorn Hall, 1190 Amsterdam Ave #406, New York, NY, USA 10027.

## How to cite:

Leshno A, Hood DC, Liebmann JM, De Moraes CG. Identifying and understanding optical coherence tomography artifacts that may be confused with glaucoma. Rev Bras Oftalmol. 2022;81:e0103.

## doi:

<https://doi.org/10.37039/1982.8551.20220103>

## Keywords:

Glaucoma; Artefatos;  
Tomography, optic coherence

## Descritores:

Glaucoma; Artefatos;  
Tomografia de coerência óptica

**Received on:**  
May 18, 2022

**Accepted on:**  
May 30, 2022

## Corresponding author:

Carlos Gustavo De Moraes, MD, MPH, PhD  
635 W 165th St, Box 69,  
Zip code: – New York, NY, 10032, USA  
E-mail: cvd2109@cumc.columbia.edu

## Institution:

Columbia University Irving Medical Center  
New York, NY, USA

## Conflict of interest:

the authors declare no conflict of interest.

## Financial support:

the authors received no financial support  
for this work.



Copyright ©2022

## ABSTRACT

Optical coherence tomography is often used for detection of glaucoma as well as to monitor progression. This paper reviews the most common types of artifacts on the optical coherence tomography report that may be confused with glaucomatous damage. We mainly focus on anatomy-related artifacts in which the retinal layer segmentation and thickness measurements are correct. In such cases, the probability maps (also known as deviation maps) show abnormal (red and yellow) regions, which may mislead the clinician to assume disease is present. This is due to the anatomic variability of the individual, and the normative database must be taken into account.

## RESUMO

A tomografia de coerência óptica é frequentemente usada para detectar glaucoma, bem como para monitorar a progressão. Este artigo analisa os tipos mais comuns de artefatos no relatório de tomografia de coerência óptica que podem ser confundidos com danos glaucomatosos. Nós nos concentramos principalmente nos artefatos relacionados à anatomia em que a segmentação da camada da retina e as medidas de espessura estão corretas. Nesses casos, os mapas de probabilidade (também conhecidos como mapas de desvio) mostram regiões anormais (vermelho e amarelo), o que pode induzir o clínico em erro ao supor que a doença está presente. Isto se deve à variabilidade anatômica do indivíduo, e o banco de dados normativo deve ser levado em conta.

## INTRODUCTION

Glaucoma clinicians use optical coherence tomography (OCT) as an important ancillary tool for the detection of glaucoma as well as monitoring its progression. Although the structural component of glaucoma damage, from a historical standpoint, has been evaluated predominantly with disc photographs and/or slit-lamp examination, these methods have poor reproducibility and poor inter-observer agreement.<sup>(1-5)</sup> The advantage of OCT lies in the high-resolution and reproducible information provided about the retinal nerve fiber (RNFL) and ganglion cell layers (GCL), which are the most relevant for glaucoma evaluation.<sup>(6-11)</sup> In addition, the test is fast, requires minimal cooperation from the patient, and results in little to no discomfort to the patient, which enables repeat testing as needed.

As with all diagnostic tests, the OCT reports can be misinterpreted due to the presence of artifacts.<sup>(12-14)</sup> In the case of summary metrics affected by artifacts, it is possible to avoid this confusion by simply ignoring them and reviewing thickness and probability/deviation maps provided in OCT reports. However, there are several types of artifacts that can affect these maps and result in changes which resemble structural damage due to glaucoma. Therefore, it is important for clinicians to become familiar with the various sources of artifacts and be able to recognize and differentiate them from actual signs of structural damage.

Here, we review the most common types of artifacts that may be confused with glaucomatous damage. In the interest of brevity, we largely ignore technical factors such as poor scan quality and errors in segmentation. Instead, we mainly focus on anatomy-related artifacts in which the retinal layer segmentation and thickness measurements are correct; however, due to its anatomic variability, which must be compared to the normative database, the probability maps (also known as deviation maps) can show abnormal (red and yellow) regions. They may lead the clinician to assume that the disease is present. Moreover, we do not discuss other retinal or neuro-ophthalmological conditions that can mimic or confuse the assessment of glaucomatous structural damage.

## GLAUCOMA-LIKE ARTIFACTS DUE TO VARIATION IN THE ANATOMY OF RETINAL NERVE FIBER BUNDLES

### An anatomical model for understanding artifacts due to variation in retinal nerve fiber bundles

To identify glaucomatous optic neuropathy (GON), we need to distinguish artifacts from those findings

characteristic of glaucomatous damage seen on the probability map. An arcuate-shaped RNFL defect is considered a hallmark of glaucomatous damage.<sup>(12)</sup> However, in some cases, normal variation in the location of the major nerve fiber bundles can create a pattern on the RNFL probability map that resembles an arcuate defect.<sup>(13,15,16)</sup> We have recently described a simple anatomical model to help understand the basis for artifacts due to misalignment of RNFL bundles.<sup>(14)</sup> Our simple model is based upon the average RNFL thickness map of healthy eyes. This map is shown in field view in figure 1A, oriented in the same way as the RNFL probability maps in the lower panels of figure 1. The black arrows indicate the average location of the major superior and inferior arcuate bundles. The black contour indicates the boundary of the thickest part of these arcuate bundles which was arbitrarily defined as the border between blue and green, an iso-thickness contour for RNFL thickness of 75 $\mu$ m. Note that the RNFL probability maps are produced by comparing local regions of an individual's RNFL thickness map to the normative RNFL thickness map. The probability maps show the results of this point-by-point comparison (with age adjustment), and the statistically significant deviation from the normative measurements are color coded as indicated below.

The black contour helps to understand the cause of arcuate-like artifacts. The probability maps indicate the statistical probability of the RNFL thickness for each location that is being decreased by a continuous color scale. In this scale, dark green is 10% and dark red, 0.1% (red and yellow indicate significantly thinner areas at 1% and 5%, respectively). If an eye had an average thickness at every location and had bundles that aligned with the average location of the healthy population, then the map would be all green. However, when the measured RNFL bundles do not align within this contour, the map is likely to produce an artifact on the probability map, despite having normal RNFL thickness. Three common causes for such misalignment are illustrated in figure 1: variation in RNFL bundle location (Figure 1B), displacement of optic disc center (Figure 1C) and cyclo-rotation due to head-tilt (Figure 1D).

Because of this contour shape, these artifacts tend to have an arcuate-like shape, which can be mistaken for glaucomatous damage. However, as illustrated in figures 1B to 1D, these arcuate-like artifacts will fall largely within the black contour derived from the average RNFL. We say "largely" because the black borders are arbitrary and could be extended slightly in order to encompass thinner regions of the average RNFL thickness. On the other hand,

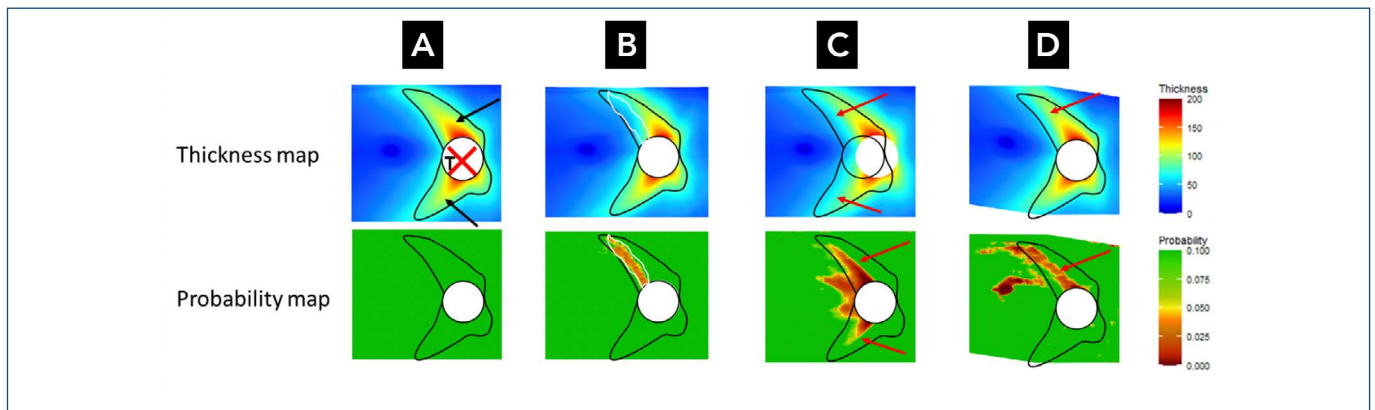


**Figure 1.** Proposed anatomical model. Simulated examples of arcuate-like artifacts due to misalignment of the average normative data with the measured retinal nerve fiber thickness. (A) Average thickness from normative data with proper alignment. (B) Simulation of nasal shift of superior retinal nerve fiber bundle. (C) Simulation of temporal shift of the disc center. (D) Simulation of cyclorotation (head tilt).

most glaucomatous arcuate-like defects are extended beyond the contour and may even cross the vertical midline of the probability map.<sup>(14)</sup> In Hood et al., we proposed that a healthy eye with an RNFL bundle of relatively normal thickness, but with an aberrant location of this bundle, will show an arcuate-like artifact on the RNFL probability map that falls within the black contour, as opposed to glaucomatous defects which usually extend outside of the contour.<sup>(14)</sup>

A detailed explanation of these three types of misalignments with case examples is described in the following sections.

### Retinal nerve fiber bundle/ blood vessel position (classic false positive)

The RNFL probability maps are produced by comparing the thickness map of the patient with that of an “average” derived from the normative database. In some eyes, there is a variation in the location of the major nerve fiber bundles – which tend to align with the major temporal blood vessels during eye development.<sup>(17-19)</sup> This variation causes misalignment with the normative data and can create a pattern on the RNFL probability map that resembles an arcuate defect as illustrated in figure 1B.<sup>(13,15)</sup> The location of the artifact will be dependent upon whether the individual’s bundles are more temporal or more nasal relative to average of the normative database and the extent of the artifact will depend on the distance between the patient’s bundles and the normative database. For example, consider the OCT reports of a 23-year-old subject in figure 2. The right eye was scanned with two OCT devices on the same day: the Triton’s Swept Source (SS) OCT (Topcon, Inc) and Heidelberg Spectralis spectral-domain (SD; Heidelberg Engineering, GmbH). In the Topcon report (Figure 2A), the

RNFL probability map shows regions in both the superior and inferior hemifield that resemble an arcuate defect. Notice, however, the close proximity between the peaks of RNFL thickness on the cpRNFL plot (black arrows). They correspond to the narrow angle between the superior and inferior RNFL bundles on the RNFL thickness map as well as thickest regions in the RNFL thickness plot (black arrows) as found in the Topcon report.

In a recent publication, La Bruna et al. found that the prevalence of such arcuate-like artifacts in healthy eyes in a normative dataset was about 5%.<sup>(16)</sup> In order to differentiate these artifacts from actual RNFL defects, they proposed the “vertical mid-line rule,” according to which an artifact arcuate-like defect would not be extended beyond the vertical mid-line of the retinal posterior pole (i.e. through the fovea). The rule was based on the known anatomical pattern of glaucomatous damage that follows an arcuate course of the damaged axons and is extended beyond the vertical midline. In comparison, arcuate artifacts that appear due to anatomical displacement of the major temporal vessels; the associated bundles of the RNFL in healthy eyes would respect the boundaries of the normal thick arcuate region.<sup>(14-15)</sup>

Consider the example in figure 2 again. Both the inferior and superior arcuate-like defects fall within the black outline and do not cross the midline (Figure 2A, see vertical dashed red line on the probability map), suggesting that these are most likely artifacts due to anatomical variation of the blood vessel position and subsequent RNFL bundles. As mentioned above, this is confirmed by normal and thick appearing RNFL on the RNFL thickness map showing close proximity between the two RNFL bundles, as well as the lack of confirmation of damage on the GCL maps.

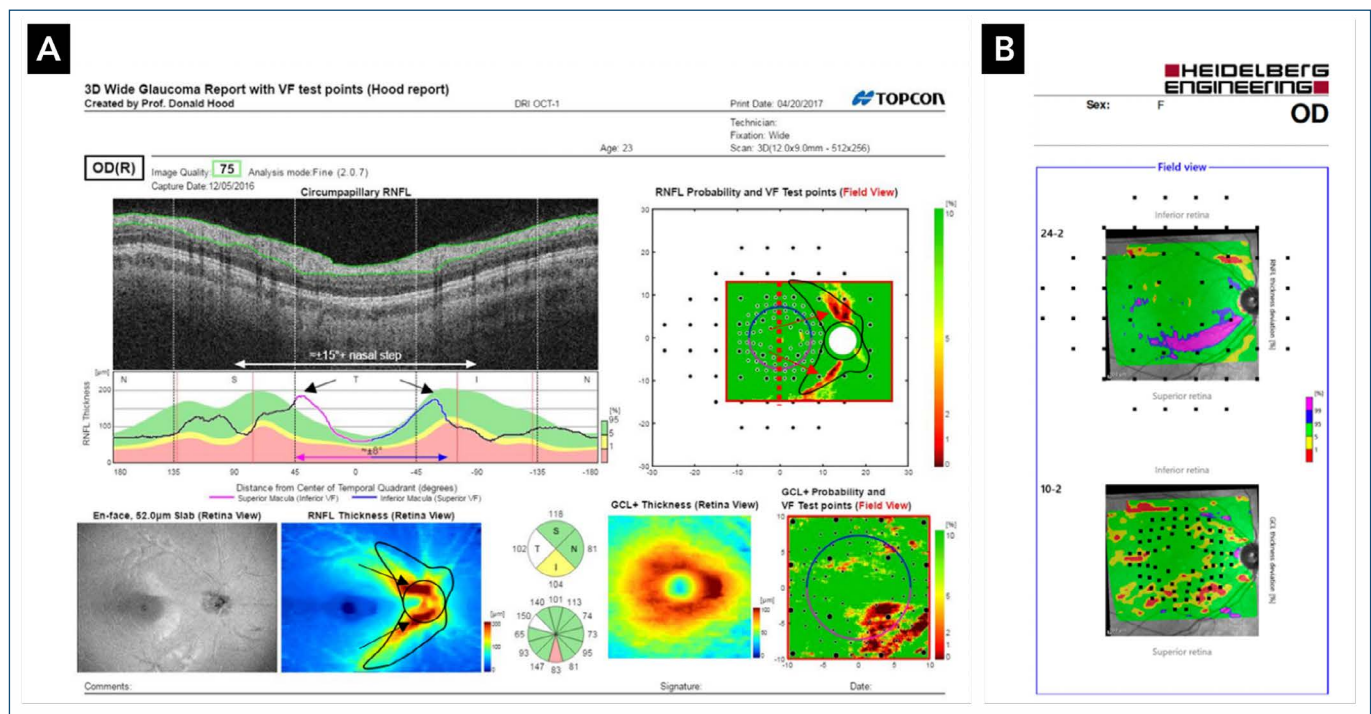


**Figure 2.** Arcuate-shaped retinal nerve fiber defects due to anatomic variation on major bundle location. (A) Topcon Hood report from a 23-year-old healthy subject scanned with the Triton Swept Source optical coherence tomography device. The retinal nerve fiber probability map shows significantly thinner arcuate-shaped areas in both the inferior and superior hemifields, resembling retinal nerve fiber defects (red arrows). However, a careful look at the retinal nerve fiber thickness map shows a relatively thick yet temporally displaced retinal nerve fiber (black arrows). The black borders on both of these maps indicate an iso-thickness ( $75\mu\text{m}$ ) border of the average thickest retinal nerve fiber around the disc. As predicted by a simple model, these arcuate-like defects in healthy eyes fall within this black border. This simple model also predicts that there should be a thicker than normal region. This can be seen to be the case in the report in B which shows significantly thicker regions. (B) Heidelberg Hood report from the same patient scanned with the Spectralis spectral-domain optical coherence tomography device on the same day. The probability maps here also show areas of significant thickening (blue-purple). Notice that in the inferior hemifield there is a “super-thick” area adjacent to the arcuate-shaped artifact. Both are due to the anatomical variation of major blood vessels and retinal nerve fiber bundles. This Hood report is available only for research purposes in some countries (e.g., the United States).

Several studies have shown a higher prevalence of temporal shift of the RNFL bundles with increasing myopia and nasal shift in hyperopia.<sup>(17,20-34)</sup> This temporal shift results in an “increase” of the temporal RNFL at the expense of the superior/inferior regions. When compared to the normative database, the “reduction” in superior/inferior RNFL thickness results in an arcuate-like artifact, as in figure 2. These artifacts stay within the black border of the region of normative RNFL and do not cross the midline. Also notice that the Heidelberg report highlights “significantly-thicker” regions on the probability map (blue-purple areas). Such an area can be seen adjacent to the area of the inferior arcuate-like defect in figure 2B (top panel), further supporting the assumption that the arcuate defect is due to an artifact.

The exact cause of the temporal shift of the RNFL bundles in myopia is not completely understood. One theory suggests that it results from temporal dragging of the retina during development or due to tilted discs, which are more common in myopic eyes.<sup>25-27,30</sup> Interestingly, there is

also a considerable variation in the location of the major temporal blood vessels as well as weaker correlation between the location of the superior and inferior vessels in myopic eyes.<sup>(20)</sup> Similar to the shift in RNFL bundles, there is also a larger temporal shift of the retinal vessels in myopic eyes, with a strong correlation between the peak of the RNFL thickness and position of the retinal arteries.<sup>(33)</sup> This finding is in part due to the contribution of the vessels themselves to the RNFL thickness measurements. Hood et al. estimated that 13% of the measured RNFL thickness is due to the blood vessels within the RNFL.<sup>(17)</sup> In addition, there is a direct connection between the RNFL and blood vessel distribution.

It should be noted that in contrast to the RNFL, the GCL layer is thought to be less affected by such anatomic variation and therefore may be more useful for evaluating eyes with large deviations in the pattern of RNFL bundles.<sup>(35)</sup> Zemorain et al. showed that OCT can be used in most cases with high myopia, usually by looking at the circumpapillary b-scan itself combined with the GCL map.<sup>(36)</sup>

## Centering

Because the OCT measurements of each eye are compared to the average layer thickness obtained from the normative database, proper alignment of the scan is critical. A misalignment of the disc center will result in a comparison between the measured thickness to an unrelated normative data-point. It is also important to note that these misalignments directly affect summary metrics by averaging the wrong regions.

The most common types of centering artifacts result from improper centering of the disc as illustrated in figure 1C. Note that changing the location of the disc center does not affect the scan itself, but rather, the reference point

based on which the comparison to the normative data is made. Several studies evaluated the effect of disc-center displacement on the cpRNFL measurements.<sup>(37-41)</sup>

Figure 3 shows an example of the artifacts due to centering. All three reports were produced from the same scan, each with different disc centering. Notice how temporal displacement of the disc center (Figure 3B) creates both inferior and superior arcuate-shaped abnormalities on the RNFL probability map. In addition, the nasal average thickness on the cpRNFL pie-chart increases to above-average-thickness at the expense of the temporal regions (especially at the 7,11 clock hours), which are reduced below the 1% percentile. A nasal displacement

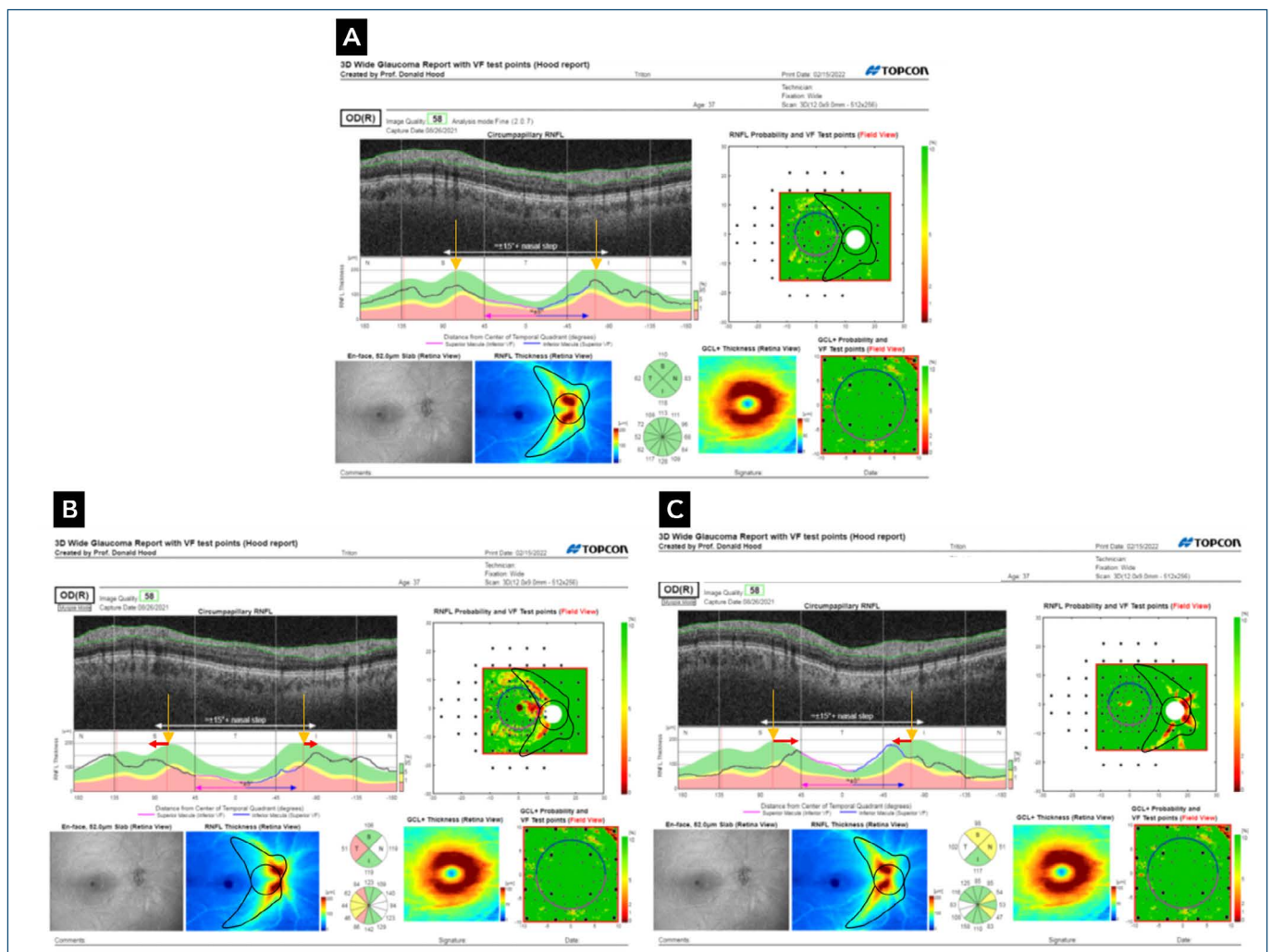


**Figure 3.** Deviation in disc centering. In order to simulate the effect of improper disc-centering on the probability map, the same scan was used to generate three different reports. In each of the three reports, the black outline indicates the location of the disc-center on the retinal nerve fiber maps (thickness and probability) defined for analysis and comparison with normative data. (A) Proper disc centering. (B) Temporal displacement of disc center resulting in both arcuate-shaped artifacts as well as temporal defects on the retinal nerve fiber probability map. Notice how the major retinal nerve fiber bundle peaks (orange arrows) move farther apart on the cpRNFL plot (red arrows) and how the average thickness on the pie-charts changes. (C) Nasal displacement of disc center resulting in a minor arcuate-shaped artifact in the inferior hemifield as well as some artifacts on the nasal half of the disc. Notice how the major retinal nerve fiber bundle peaks (orange arrows) move closer to each other on the cpRNFL plot (red arrows).

(Figure 3C) by a similar extent creates a more subtle artifact on the RNFL probability map. Notice how in both cases of displacement, most of the artifact falls within the black border, similar to the arcuate-like artifacts that result from variation in bundle position (discussed in the previous section). The displacement is also evident in the cpRNFL thickness plot where the two highest peaks on the RNFL are much closer in the plot after nasal displacement and farther apart after temporal displacement, compared to their distance in the report with proper centering. Note that in all three reports, the thickness map of the RNFL remains the same and shows a normal thickness pattern which is consistent with the probability map with correct centering of the disc (Figure 3A).

In general, vertical displacement of the disc center affects mostly the superior and inferior sectors of the cpRNFL thickness, and horizontal displacement primarily affects the nasal and temporal sectors; that is, increasing the average thickness in the sector that is in the same direction as the shift at the expense of the opposite sector. Nasal displacement also has a more significant effect on global thickness.<sup>(41)</sup>

Gabriele et al. found that horizontal shifts also affected the distance between the two peaks of the cpRNFL thickness plot, which was greater with nasal displacement and smaller with temporal displacement.<sup>(38)</sup> These types of misalignments should be detected during scan acquisition by the technician, and then the centering should be corrected manually or the scan repeated. In any case, these shifts usually can be identified on the OCT report by looking at the thickness map, which will show a deviation of the scan area.

### Rotational misalignment due to fovea-to-disc angle and cyclotorsion

Even when the disc-center is properly aligned, there can still be misalignment due to rotation of the scan, as illustrated in figure 1D. For example, consider the two OCT reports shown in figure 4, from a 26-year-old healthy individual. The first report (Figure 4A) shows a normal RNFL thickness without any significant areas of abnormal thinning on the probability map. On the subsequent scan, taken less than 2 months after the initial scan, an arcuate-shaped defect appears on the superior hemifield, suggesting progression. However, the RNFL thickness seems to be nearly identical in both scans. A careful comparison shows that the scan on the second visit is slightly rotated counterclockwise. This explains the observed changes on the RNFL probability map. Also notice that the cpRNFL

thickness remains very similar on both scans, with only a slight shift to the right (yellow arrow).

The most significant cause for rotation misalignment is due to eye cyclotorsion, from either head tilt or strabismus. A head tilt results in fast transient torsional eye movement during scan acquisition.<sup>(42-44)</sup> Although this is followed by an immediate compensatory movement of the eye towards the initial baseline position, the physiologic relative torsion compensation ranges only between 13% and 22%.<sup>(44)</sup> Therefore, it is not always sufficient to correct the eye movements induced by the head tilt. This can be particularly significant among patients with strabismus, especially those suffering from conditions that involve the oblique muscles (e.g., superior oblique palsy, skew deviation).

Due to the nature of the shift, the thickness measurements move depending on the direction of the head and eye: a tilt to the right results with incyclotorsion of the right eye and excyclotorsion of the left eye. Hwang et al. showed that head tilt induced counterclockwise ~8-degree rotation of the optic disc on average among healthy controls scanned with the Cirrus HD OCT (Carl Zeiss, Inc). This change significantly affected both RNFL and macular sector thickness metrics.<sup>(45)</sup>

Another common cause of rotation misalignment comes from anatomic variability among individuals in the position of the center of the fovea relative to the disc commonly expressed by the fovea-to-disc angle. As previously shown, there is considerable variability among individuals in this angle. For example, in the Beijing Eye Study 2011, a population-based cross-sectional study including 3,468 individuals, the mean disc-fovea angle was  $7.76 \pm 3.63^\circ$  (median:  $7.65^\circ$ ; range:  $-6.3^\circ$  to  $28.9^\circ$ ).<sup>(46)</sup> The mean inter-eye difference was  $4.01 \pm 2.94^\circ$  (median:  $3.49^\circ$ ; range:  $0.00$ – $22.3^\circ$ ). Hood et al. also reported that the average angle of vertical displacement of the center of the disc was  $6.3^\circ$  above the center of the fovea but can range from  $-1.95^\circ$  below the center of the fovea to  $13.96^\circ$  above.<sup>(47)</sup> The horizontal distance between the center of the fovea and the disc has a narrower range, from  $11.79$  to  $16.93^\circ$ , with an average of  $14.8^\circ$ . However, these measurements were also affected by possible head torsion.

Both cyclorotation and fovea-to-disc angles can contribute to incorrect comparisons to the machine normative database and affect both summary metrics and probability maps. This is also important in terms of repeatability of the RNFL and GCL measurements as the torsion can vary between scans and visits, which the clinician might wrongly attribute to progression, as in the

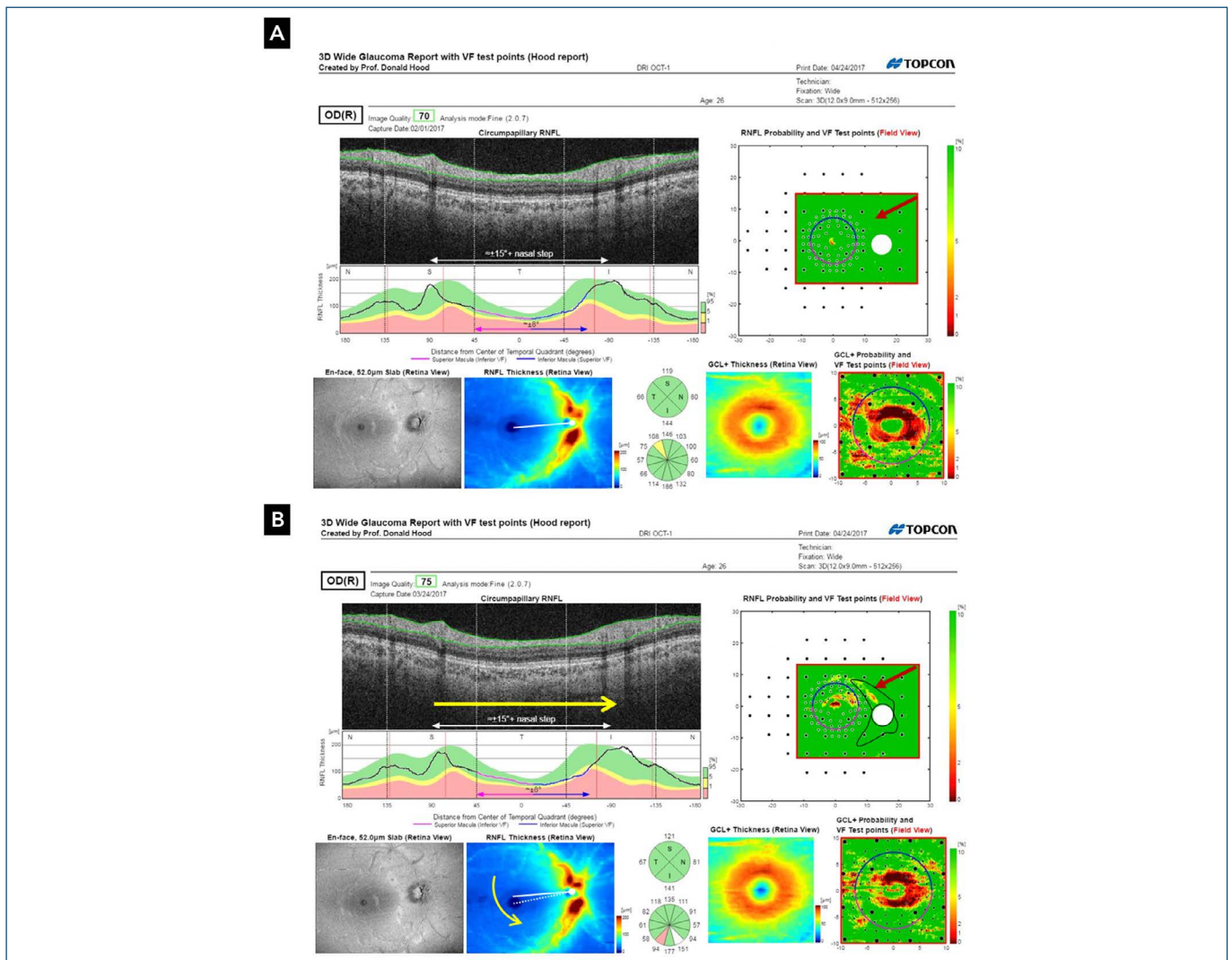


**Figure 4.** Artifacts due to uncorrected cyclotorsion/ head tilt. (A) Report of a healthy 26-year-old individual showing a normal retinal nerve fiber thickness map. (B) In a subsequent visit, an arcuate-shaped retinal nerve fiber defect appears in the superior hemifield (red arrow) suggesting progression (note also the red in the 7<sup>th</sup> clock-hour pie chart corresponding to the same location). However, a more careful examination reveals that the retinal nerve fiber thickness did not change except for some counter-clockwise rotation, which resulted in an increase of the fovea-to-disc angle (white lines). Notice also that the cpRNFL thickness line remained the same, but the thickness map appears to have shifted slightly to the right (horizontal yellow arrow). This was most likely due to head-tilt and cyclotorsion, which resulted in the observed artifact. Moreover, most of the artifact falls within the black outline as predicted by the anatomical model.<sup>(14)</sup>

example in figure 4. However, some OCT devices automatically correct for such misalignment issues. For example, the Spectralis (Heidelberg Engineering, GmbH) automatically tilts the scanning angle to match the fovea-to-disc angle, measured during the baseline scan, in an attempt to minimize the effect of the anatomic variation among individuals. The effect of the fovea-to-disc angle is relatively small due to the fact that this technique forces the scan angle to be constant throughout all scan sessions. In spite of this, it is also effective in minimizing the effect of possible cyclotorsion due to head tilt. Ismail et al. compared the effect of head tilt in healthy individuals on two SD-OCT devices: the Cirrus (Carl Zeiss, Inc.) and

the Spectralis (Heidelberg Engineering, GmbH).<sup>(48)</sup> At that time, only the Spectralis had a fovea-to-disc alignment technology aimed to overcome errors originating from changes in head/eye position or anatomical variations. The study showed that while head tilt significantly affected the cpRNFL thickness measurements on the Cirrus, the effect on the Spectralis was minimal and insignificant.

The artifacts produced by this type of misalignment can resemble glaucomatous arcuate-shaped defects on the RNFL probability map as illustrated in figure 1D and in the case example of figure 4. Considering that both the inferior and superior RNFL bundles transpose as a result of the head tilt, an area with thinner RNFL would be

compared to the thickest portion of the RNFL on the normative data. As a result, the major RNFL bundles might be considered significantly below average, depending on the overall RNFL thickness in that region with the potential to create a superior and/or inferior arcuate-like patterns depending on the direction of the rotation. For example, in figure 4 an incyclorotation (counterclockwise, curved yellow arrow in figure 4B) resulted in a superior arcuate.

Artifacts due to rotation will fall mostly within the black contour and respect the midline rule as described above for artifacts due to aberrant location of the RNFL bundle, or displacement of the disc-center. These artifacts should be suspected when the peaks on the cpRNFL plot do not correspond to the peaks of the normative database.

## ADDITIONAL ARTIFACTS DUE TO ANATOMIC VARIATIONS

### Variation in foveal anatomy

Although in the past it was generally believed that central field damage from glaucoma occurred only in the later stages of the disease process, various studies have shown that central damage (corresponding to the macula) can occur in early stages of the disease.<sup>(47)</sup> However, anatomical variation of the macular region (defined here within  $\pm 8^\circ$  from fixation) between individuals can also produce artifacts. Consider for example the OCT scan from a healthy 67-year-old individual shown in figure 5A. Note that the cpRNFL looks thick and healthy without any areas of significant thinning highlighted on the RNFL probability map or cpRNFL plot. However, the GCL probability map shows a ring-shaped area of thinning located within the central 5 degrees (red arrow). Also note that this “defect” is quite uniform and that there are no clear signs of focal damage on the GCL thickness map. Visual field tests (both 24-2 and 10-2 conducted on the same day as the scan) confirm that there is no functional damage. This is an example of a ring artifact due to anatomical variation in healthy eyes, as described by De Moraes et al.<sup>(49)</sup>

An abnormal probability GCL map should be scrutinized and correlated with the RNFL maps, clinical exam, and functional tests. The slope and depth of the foveal depression, as well as the overall GCL thickness, show inter-individual variation that can result in circular or partial circular abnormal regions on the GCL probability maps.

It is important to ensure that the fovea was correctly identified and centered by the OCT analysis; otherwise, artifactual thickening and thinning of the retina will be displayed as abnormal (red arrow, Figure 5B). Even with correct centering, artifacts such as that shown in figure

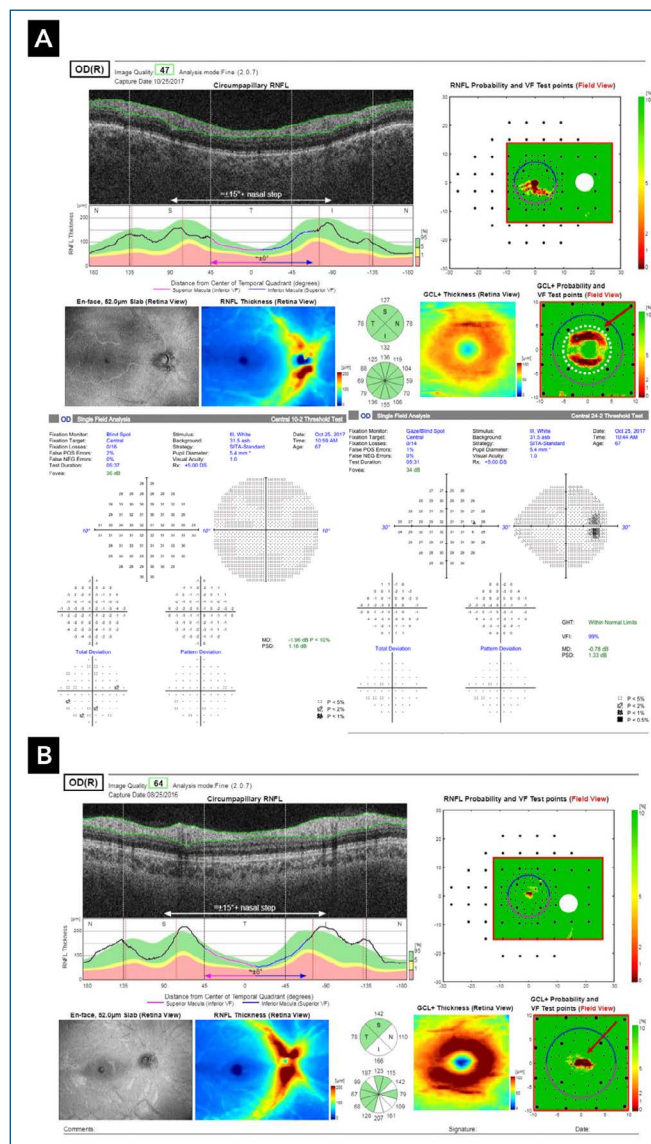


**Figure 5.** Example of a circum-foveal artifact. (A) Circum-foveal artifact: “abnormal” regions ( $< 1\%$ , red) largely within the central  $\pm 4^\circ$  (white dashed circle) in both hemi-retinas. Both 24-2 and 10-2 visual field test performed on the same day as the scan verify that there is no functional abnormality scan. (B) Example of central foveal dot-artifact (red arrow) in an otherwise normal.

5A can occur. However, true atrophy of the GCL + inner plexiform layer (IPL) may also cause perifoveal thinning and enlargement of the foveal depression. This may hinder differentiation of focal pathological thinning in the perifoveal inner retina compared to normal variation in thickness in this location.

In general, it is important to always check for consistency with the rest of the report. A GCL abnormality that matches an anatomically corresponding RNFL arcuate defect is less likely to be due to anatomical artifacts than one in which there is agreement. In addition, it is strongly recommend to evaluate individual b-scans of the macula,



especially when artifacts are suspected, to rule out retinal abnormalities, as well as to help distinguish between glaucoma versus other optic neuropathies.<sup>15,47</sup>

### Incorrect input of patient age

The probability maps on the OCT report depend upon a comparison to an age-adjusted normative data to account for the changes in RNFL thickness that occur with normal aging. Consequently, if the date of birth is incorrectly entered, this can create artifacts, including exaggerating the degree of the actual damage. For example, consider the GCL probability map in Figure 6 taken from a healthy 73-year-old individual. At first (Figure 6A), the wrong date of birth was entered, falsely changing the subject's age to 22 years during scanning. This made it seem that there was a significant thinning of the GCL, especially within the superior hemiretina. However, after correcting the date of birth to the actual age of 73, the significant thinning of the GCL nearly disappeared (Figure 6B).

### Lower end of normal

It is challenging to differentiate eyes with diffuse glaucomatous damage from healthy eyes in which the measurements fall within the bottom fifth percentile of the distribution of normative database. Thus, some individuals born with an RNFL thickness at the lower end of normal range may reveal abnormalities on probability

maps. Consider, for example, the two reports provided in figure 7. Although one is from a scan of a healthy eye (A) and the other from an eye with advanced glaucoma (B), at first look, both reports look very similar, with an almost identical pattern of mostly temporal thinning on the RNFL probability map and the cpRNFL thickness plot. Even though it is based on the RNFL thickness map, it can often be difficult to determine which eye is healthy and which suffered from diffuse damage.

In unilateral cases, it might be possible to identify glaucomatous axonal loss based upon interocular asymmetry. If one assumes that both eyes had similar RNFL and GCL thickness at birth, a significant difference might indicate that the eye with thinner RNFL and/or GCL has been damaged. However, this type of comparison is challenging, especially if both eyes have glaucomatous damage.

The GCL thickness map can also help in differentiating such difficult cases. Although eyes with diffuse glaucomatous damage and healthy eyes in the lower end of the normal range will have thin RNFL and GCL, the GCL of the glaucomatous eye often has a patchy pattern of loss.<sup>14</sup> Consider the two GCL thickness maps in figure 7. Both are significantly thinner compared to the normative data, as shown in the GCL probability maps; however, while the GCL thickness map in figure 7A of the healthy eye looks uniformly thin, the one in Figure 7B of the glaucomatous eye seems patchy with more inferior than superior thinning. While we cannot be sure

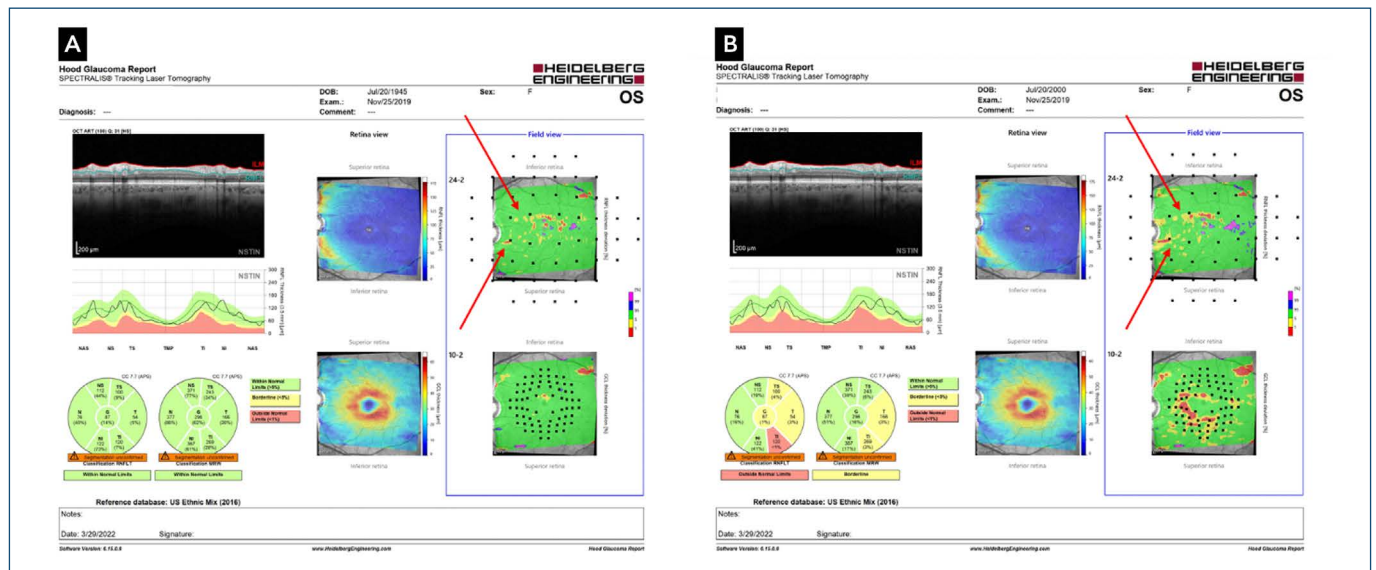


**Figure 6.** Artifacts due to an incorrect date of birth. Heidelberg optical coherence tomography report of a healthy 73 year old patient. (A) The report with the proper date of birth showing a normal appearing retinal nerve fiber and ganglion cell layers without any significantly thin areas on the probability maps. (B) The same scan but the report produced with the wrong date of birth, making the patient “younger” by 51 years (22 instead of 73). Notice the temporal retinal nerve fiber “defects” (red arrows) become thicker and more obvious with a more significant change on the ganglion cell layers probability map. The cpRNFL pie chart also becomes yellow and red in the temporal half.

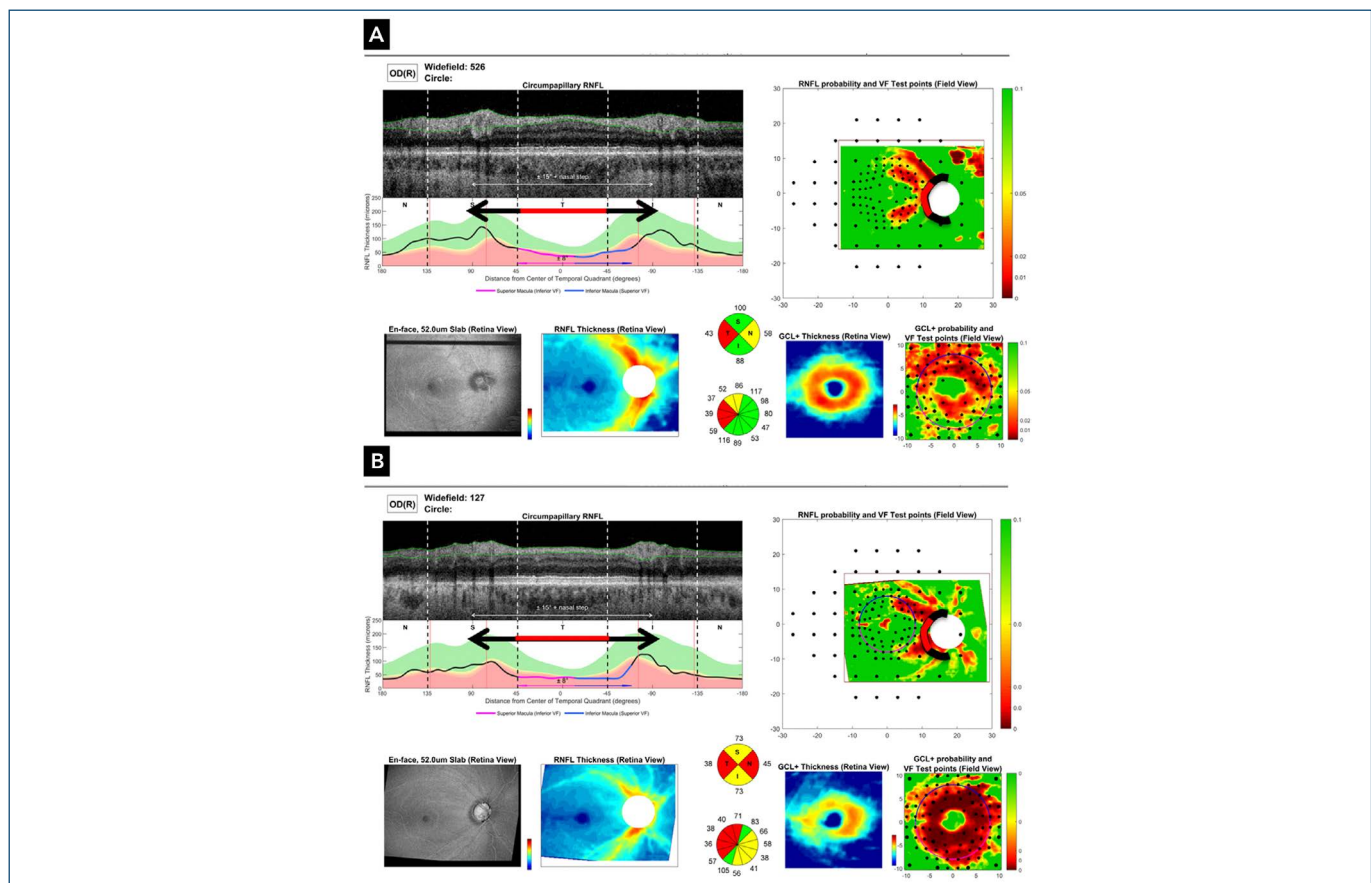


**Figure 7.** Lower end of normal. Example of the difficulty in differentiating, glaucoma from healthy eyes that fall within the lower fifth percentile of the normative database. The optical coherence tomography reports taken from two different individuals show very similar patterns on the retinal nerve fiber probability map (top right) and cpRNFL thickness plot (top left). Even though it is based on the retinal nerve fiber thickness map, it is hard to determine which eye is healthy and which one suffers from diffuse damage. However, a closer look at the ganglion cell layers thickness reveals that while the healthy eye has a rather uniform ganglion cell layers (A), the glaucomatous eye (B) has a patchy pattern, suggesting areas of focal damage.

that the eye with the uniformly thin GCL is healthy, we can be reasonably sure the one with the patchy loss of the GCL is not. Recently, Zemborain et al. suggested a metric based upon a comparison of the cpRNFL thickness profile to differentiate the two groups.<sup>(50)</sup> However, this technique is not commercially-available. Although it was successful in the vast majority of cases, some glaucomatous eyes were still missed.

## COMMENTS

Without scanning artifacts or segmentation errors, optical coherence tomography reports can show artifacts due to normal anatomical variations and/or centering mistakes. We describe a simple anatomical mode<sup>(14)</sup> and rules that need to be followed to avoid mistakenly diagnosing glaucoma or incorrectly assessing severity. In particular, the clinician should evaluate all components of an OCT report, as well as the topographical correlation between the different portions of the report.<sup>(15)</sup>

## REFERENCES

1. Lichter PR. Variability of expert observers in evaluating the optic disc. *Trans Am Ophthalmol Soc.* 1976;74:532-72.
2. Cooper R, Alder V, Constable I. Measurement vs. judgement of cup-disc ratios: statistical evaluation of intraobserver and interobserver error. *Glaucoma.* 1982;4:169-76.
3. Tielsch JM, Katz J, Quigley HA, Miller NR, Sommer A. Intraobserver and interobserver agreement in measurement of optic disc characteristics. *Ophthalmology.* 1988;95(3):350-6.
4. Abrams LS, Scott IU, Spaeth GL, Quigley HA, Varma R. Agreement among optometrists, ophthalmologists, and residents in evaluating the optic disc for glaucoma. *Ophthalmology.* 1994;101(10):1662-7.
5. Zangwill LM, Shakiba S, Caprioli J, Weinreb RN. Agreement between clinicians and a confocal scanning laser ophthalmoscope in estimating cup/disk ratios. *Am J Ophthalmol.* 1995;119(4):415-21.
6. Schuman JS, Pedut-Kloizman T, Hertzmark E, Hee MR, Wilkins JR, Coker JG, et al. Reproducibility of nerve fiber layer thickness measurements using optical coherence tomography. *Ophthalmology.* 1996;103(11):1889-98.
7. Blumenthal EZ, Williams JM, Weinreb RN, Girkin CA, Berry CC, Zangwill LM. Reproducibility of nerve fiber layer thickness measurements by use of optical coherence tomography. *Ophthalmology.* 2000;107(12):2278-82.
8. Carpineto P, Ciancaglini M, Zuppardi E, Falconio G, Doronzo E, Mastropasqua L. Reliability of nerve fiber layer thickness measurements using optical coherence tomography in normal and glaucomatous eyes. *Ophthalmology.* 2003;110(1):190-5.

9. Budenz DL, Fredette MJ, Feuer WJ, Anderson DR. Reproducibility of peripapillary retinal nerve fiber thickness measurements with stratus OCT in glaucomatous eyes. *Ophthalmology*. 2008;115(4):661-6.e4.
10. Mwanza JC, Chang RT, Budenz DL, Durbin MK, Gendy MG, Shi W, et al. Reproducibility of peripapillary retinal nerve fiber layer thickness and optic nerve head parameters measured with Cirrus HD-OCT in glaucomatous eyes. *Invest Ophthalmol Vis Sci*. 2010;51(11):5724-30.
11. Langenegger SJ, Funk J, Töteberg-Harms M. Reproducibility of retinal nerve fiber layer thickness measurements using the eye tracker and the retest function of spectralis SD-OCT in glaucomatous and healthy control eyes. *Invest Ophthalmol Vis Sci*. 2011;52(6):3338-44.
12. Chong GT, Lee RK. Glaucoma versus red disease: imaging and glaucoma diagnosis. *Curr Opin Ophthalmol*. 2012;23(2):79-88.
13. Chen JJ, Kardon RH. Avoiding clinical misinterpretation and artifacts of optical coherence tomography analysis of the optic nerve, retinal nerve fiber layer, and ganglion cell layer. *J Neuroophthalmol*. 2016;36(4):417-38.
14. Hood DC, La Bruna S, Tsamis E, Thakoor KA, Rai A, Leshno A, et al. Detecting glaucoma with only OCT: Implications for the clinic, research, screening, and AI development. *Prog Retin Eye Res*. 2022;101052.
15. Hood DC. Improving our understanding, and detection, of glaucomatous damage: An approach based upon optical coherence tomography (OCT). *Prog Retin Eye Res*. 2017;57:46-75.
16. La Bruna S, Rai A, Mao G, Kerr J, Amin H, Zemborain ZZ, et al. The OCT RNFL probability map and artifacts resembling glaucomatous damage. *Transl Vis Sci Technol*. 2022;11(3):18.
17. Hood DC, Fortune B, Arthur SN, Xing D, Salant JA, Ritch R, et al. Blood vessel contributions to retinal nerve fiber layer thickness profiles measured with optical coherence tomography. *J Glaucoma*. 2008;17(7):519-28.
18. Hood DC, Salant JA, Arthur SN, Ritch R, Liebmann JM. The location of the inferior and superior temporal blood vessels and interindividual variability of the retinal nerve fiber layer thickness. *J Glaucoma*. 2010;19(3):158-66.
19. Qiu K, Schiefer J, Nevalainen J, Schiefer U, Jansonius NM. Influence of the retinal blood vessel topography on the variability of the retinal nerve fiber bundle trajectories in the human retina. *Invest Ophthalmol Vis Sci*. 2015;56(11):6320-5.
20. Hougaard JL, Ostenfeld C, Heijl A, Bengtsson B. Modelling the normal retinal nerve fibre layer thickness as measured by Stratus optical coherence tomography. *Graefes Arch Clin Exp Ophthalmol*. 2006;244(12):1607-14.
21. Sharma N, Sony P, Gupta A, Vajpayee RB. Effect of laser in situ keratomileusis and laser-assisted subepithelial keratectomy on retinal nerve fiber layer thickness. *J Cataract Refract Surg*. 2006;32(3):446-50.
22. Leung CK, Cheng AC, Chong KK, Leung KS, Mohamed S, Lau CS, et al. Optic disc measurements in myopia with optical coherence tomography and confocal scanning laser ophthalmoscopy. *Invest Ophthalmol Vis Sci*. 2007;48(7):3178-83.
23. Rauscher FM, Sekhon N, Feuer WJ, Budenz DL. Myopia affects retinal nerve fiber layer measurements as determined by optical coherence tomography. *J Glaucoma*. 2009;18(7):501-5.
24. Hong S, Kim CY, Seong GJ. Adjusted peripapillary retinal nerve fiber layer thickness measurements based on the optic nerve head scan angle. *Invest Ophthalmol Vis Sci*. 2010;51(8):4067-74.
25. Hong SW, Ahn MD, Kang SH, Im SK. Analysis of peripapillary retinal nerve fiber distribution in normal young adults. *Invest Ophthalmol Vis Sci*. 2010;51(7):3515-23.
26. Kang SH, Hong SW, Im SK, Lee SH, Ahn MD. Effect of myopia on the thickness of the retinal nerve fiber layer measured by cirrus HD optical coherence tomography. *Invest Ophthalmol Vis Sci*. 2010;51(8):4075-83.
27. Kim MJ, Lee EJ, Kim TW. Peripapillary retinal nerve fibre layer thickness profile in subjects with myopia measured using the Stratus optical coherence tomography. *Br J Ophthalmol*. 2010;94(1):115-20.
28. Wang G, Qiu KL, Lu XH, Sun LX, Liao XJ, Chen HL, et al. The effect of myopia on retinal nerve fibre layer measurement: a comparative study of spectral-domain optical coherence tomography and scanning laser polarimetry. *Br J Ophthalmol*. 2011;95(2):255-60.
29. Hwang YH, Yoo C, Kim YY. Characteristics of peripapillary retinal nerve fiber layer thickness in eyes with myopic optic disc tilt and rotation. *J Glaucoma*. 2012;21(6):394-400.
30. Hwang YH, Yoo C, Kim YY. Myopic optic disc tilt and the characteristics of peripapillary retinal nerve fiber layer thickness measured by spectral-domain optical coherence tomography. *J Glaucoma*. 2012;21(4):260-5.
31. Savini G, Barboni P, Parisi V, Carbonelli M. The influence of axial length on retinal nerve fibre layer thickness and optic-disc size measurements by spectral-domain OCT. *Br J Ophthalmol*. 2012;96(1):57-61.
32. Yoo YC, Lee CM, Park JH. Changes in peripapillary retinal nerve fiber layer distribution by axial length. *Optom Vis Sci*. 2012;89(1):4-11.
33. Yamashita T, Asaoka R, Tanaka M, Kii Y, Yamashita T, Nakao K, et al. Relationship between position of peak retinal nerve fiber layer thickness and retinal arteries on sectoral retinal nerve fiber layer thickness. *Invest Ophthalmol Vis Sci*. 2013;54(8):5481-8.
34. Yamashita T, Kii Y, Tanaka M, Yoshinaga W, Yamashita T, Nakao K, et al. Relationship between supernormal sectors of retinal nerve fibre layer and axial length in normal eyes. *Acta Ophthalmol*. 2014;92(6):e481-7.
35. Lee KH, Kim CY, Kim NR. Variations of retinal nerve fiber layer thickness and ganglion cell-inner plexiform layer thickness according to the torsion direction of optic disc. *Invest Ophthalmol Vis Sci*. 2014;55(2):1048-55.
36. Zemborain ZZ, Jarukasetphon R, Tsamis E, De Moraes CG, Ritch R, Hood DC. Optical coherence tomography can be used to assess glaucomatous optic nerve damage in most eyes with high myopia. *J Glaucoma*. 2020;29(10):833-45.
37. Campbell RJ, Coupland SG, Buhmann RR, Kertes PJ. Effect of eccentric and inconsistent fixation on retinal optical coherence tomography measures. *Arch Ophthalmol*. 2007;125(5):624-7.
38. Gabriele ML, Ishikawa H, Wollstein G, Bilonick RA, Townsend KA, Kagemann L, et al. Optical coherence tomography scan circle location and mean retinal nerve fiber layer measurement variability. *Invest Ophthalmol Vis Sci*. 2008;49(6):2315-21.
39. Vizzeri G, Bowd C, Medeiros FA, Weinreb RN, Zangwill LM. Effect of improper scan alignment on retinal nerve fiber layer thickness measurements using stratus optical coherence tomograph. *J Glaucoma*. 2008;17(5):341-9.
40. Yoo C, Suh IH, Kim YY. The influence of eccentric scanning of optical coherence tomography on retinal nerve fiber layer analysis in normal subjects. *Ophthalmologica*. 2009;223(5):326-32.
41. Shin JW, Shin YU, Uhm KB, Sung KR, Kang MH, Cho HY, et al. The effect of optic disc center displacement on retinal nerve fiber layer measurement determined by spectral domain optical coherence tomography. *PLOS ONE*. 2016;11(10):e0165538.
42. Pansell T, Schworm HD, Ygge J. Torsional and vertical eye movements during head tilt dynamic characteristics. *Invest Ophthalmol Vis Sci*. 2003;44(7):2986-90.
43. Pansell T, Ygge J, Schworm HD. Conjugacy of Torsional Eye Movements in Response to a Head Tilt Paradigm. *Invest Ophthalmol Vis Sci*. 2003;44(6):2557-64.
44. Schworm HD, Ygge J, Pansell T, Lennerstrand G. Assessment of ocular counterroll during head tilt using binocular video oculography. *Invest Ophthalmol Vis Sci*. 2002;43(3):662-7.
45. Hwang YH, Lee JY, Kim YY. The effect of head tilt on the measurements of retinal nerve fibre layer and macular thickness by spectral-domain optical coherence tomography. *Br J Ophthalmol*. 2011;95(11):1547-51.
46. Jonas RA, Wang YX, Yang H, Li JJ, Xu L, Panda-Jonas S, et al. Optic disc - fovea angle: The Beijing Eye Study 2011. *PLOS ONE*. 2015;10(11):e0141771.
47. Hood DC, Raza AS, Moraes CG, Liebmann JM, Ritch R. Glaucomatous damage of the macula. *Prog Retin Eye Res*. 2013;32:1-21.
48. Bin Ismail MA, Hui Li Lilian K, Yap SC, Yip LW. Effect of head tilt and ocular compensatory mechanisms on retinal nerve fiber layer measurements by cirrus spectral domain and spectralis optical coherence tomography in normal subjects. *J Glaucoma*. 2016;25(7):579-83.
49. De Moraes CG, Muhammad H, Kaur K, Wang D, Ritch R, Hood DC. Interindividual variations in foveal anatomy and artifacts seen on inner retinal probability maps from spectral domain OCT scans of the macula. *Transl Vis Sci Technol*. 2018;7(2):4.
50. Zemborain ZZ, Tsamis E, La Bruna S, Leshno A, De Moraes CG, Ritch R, et al. Distinguishing healthy from glaucomatous eyes with OCT global circumpapillary retinal nerve fiber (cpRNFL) thickness in the bottom 5th percentile. *J Glaucoma*. 2022 Mar 18.